BLED WORKSHOPS
IN PHYSICS
VOL. 19, NO. 2

Proceedings to the 21*st Workshop*
What Comes Beyond . . . *(p. 27)*
Bled, Slovenia, June 23–July 1, 2018

2 New Model independent Results From the First Six Full Annual Cycles of DAMA/LIBRA–Phase2

R. Bernabei[1], P. Belli[1], A. Bussolotti[1], R. Cerulli[1],
A. Di Marco[1], V. Merlo[1], F. Montecchia[1]***,
F. Cappella[2], A. d'Angelo[2], A. Incicchitti[2], A. Mattei[2],
V. Caracciolo[3],
C.J. Dai[4], H.L. He[4], X.H. Ma[4],
X.D. Sheng[4], Z.P. Ye[4]†

[1]Dip. di Fisica, Università di Roma "Tor Vergata" and
INFN, sez. Roma "Tor Vergata", Rome, Italy
[2]Dip. di Fisica, Università di Roma "La Sapienza" and
INFN, sez. Roma, Rome, Italy
[3]Laboratori Nazionali del Gran Sasso
I.N.F.N., Assergi, Italy
[4]Key Laboratory of Particle Astrophysics
IHEP, Chinese Academy of Sciences, Beijing, China

Abstract. New model-independent results from the first six full annual cycles of DAMA/LIBRA–phase2 (total exposure of 1.13 ton × yr) are presented. The new improved DAMA/LIBRA–phase2 experimental configuration ($\simeq$ 250 kg highly radio-pure NaI(Tl) with new HAMAMATSU high quantum efficiency photomultipliers and new electronics) allowed lower software energy threshold down to 1 keV. The DAMA/LIBRA–phase2 data confirm the evidence of a signal that meets all the requirements of the model independent Dark Matter (DM) annual modulation signature, at 9.5 σ C.L. in the (1–6) keV energy range. In the (2–6) keV energy range, considering all together the data of DAMA/NaI, DAMA/LIBRA–phase1 and DAMA/LIBRA–phase2 (total exposure 2.46 ton × yr, collected over 20 annual cycles with three different set-ups), the achieved C.L. is 12.9 σ. No systematics or side reaction able to mimic the exploited DM signature (i.e. to account for the whole measured modulation amplitude and to simultaneously satisfy all the requirements of the signature), has been found or suggested by anyone throughout some decades thus far.

Povzetek. Avtorji predstavijo nove rezultate meritev iz obdobja prvih šest let na experientu DAMA/LIBRA - faza 2 (z ekspozicijo 1.13 ton ×šest let). Poskrbijo, da so rezultati meritev neodvisni od izbire modela za opis dogodkov.

Izboljšana izvedba poskusa — z $\simeq$ 250 kg visoko čistega Na(Tl), z novimi fotopomnoževalkami Hamamatsu z višjim kvantnim izkoristkom ter izboljšano elektroniko — je omogočila, da so energijski prag znižali na 1 keV. Tudi te meritve potrdijo obstoj signala z letno modulacijo z zanesljivostjo 9.5 σ v območju energij (1–6) keV. Ko združijo

*** *also Dip. di Ingegneria Civile e Ingegneria Informatica, Università di Roma "Tor Vergata", Rome, Italy*

† *also University of Jinggangshan, Jiangxi, China*

v območju energij (2–6) keV meritve vseh dosedanjih poskusov v več kot 20 letih, to je poskusov DAMA/NaI, DAMA/LIBRA-faza1 in DAMA/LIBRA-faza2, ki doseže kupaj ekspozicijo 2.46 ton $\times$ let, dosežejo zanesljivost 12.9 σ. Nikomur dosedaj, bodisi v skupini DAMA/LIBRA bodisi v katerikoli drugi skupini, ni uspelo najti drugega pojasnila za ta izmerjeni signal, kot da ga povzroča temne snovi.

Keywords: dark matter detection, experiment, annual modulation signature, galactic dark halo, DAMA/LIBRA

2.1 Introduction

The DAMA/LIBRA [1–12] experiment, as the former DAMA/NaI [10,13–17], investigates the presence of DM particles in the galactic halo by exploiting the DM annual modulation signature (originally suggested in Ref. [18,19]). The developed highly radio-pure NaI(Tl) target-detectors [1,6,9,20] offer sensitivity to a wide range of DM candidates, interaction types and astrophysical scenarios (see e.g. in [10] and in literature).

The DM annual modulation signature and its peculiar features are linked to to the Earth motion with respect to the DM particles constituting the Galactic Dark Halo; thus, it is not related to terrestrial seasons. In fact as a consequence of the Earth's revolution around the Sun, which is moving in the Galaxy with respect to the Local Standard of Rest toward the star Vega near the constellation of Hercules, the Earth should be crossed by a larger flux of DM particles around $\simeq$ 2 June (when the Earth orbital velocity is summed to that of the solar system with respect to the Galaxy) and by a smaller one around $\simeq$ 2 December (when the two velocities are subtracted). In particular, the effect induced by DM particles must simultaneously satisfy all the following requirements: the rate must contain a component modulated according to a cosine function (1) with one year period (2) and a phase that peaks roughly $\simeq$ 2 June (3); this modulation must only be found in a well-defined low energy range, where DM particle induced events can be present (4); it must apply only to those events in which just one detector of many actually "fires" (*single-hit* events), since the DM particle multi-interaction probability is negligible (5); the modulation amplitude in the region of maximal sensitivity must be $\lesssim$7% for usually adopted halo distributions (6), but it can be larger in case of some proposed scenarios such as e.g. those in Ref. [21–25] (even up to $\simeq$ 30%). Thus, this signature is very distinctive, has many peculiarities and allows to test a wide range of parameters in many possible astrophysical, nuclear and particle physics scenarios.

This DM signature might be mimicked only by systematic effects or side reactions able to account for the whole observed modulation amplitude and to simultaneously satisfy all the requirements given above; none able to do that has been found or suggested by anyone throughout some decades thus far [1–5,7,8,10,15–17].

The data of the former DAMA/NaI setup and, later, those of the DAMA/LIBRA–phase1 have already given positive evidence with high confidence level for the

presence of a signal that satisfies all the requirements of the exploited DM signature [2–5,10,16,17]. Here the model independent result of six full annual cycles of DAMA/LIBRA–phase2 is presented [12]. The total exposure of DAMA/LIBRA–phase2 is: 1.13 ton $\times$ yr with an energy threshold at 1 keV. When including also that of the first generation DAMA/NaI experiment and of DAMA/LIBRA–phase1 the cumulative exposure is 2.46 ton $\times$ yr. Details on the annual cycles of DAMA/LIBRA–phase2 are reported in Ref. [12]; in particular, the total number of events collected for the energy calibrations during DAMA/LIBRA–phase2 is about 1.3×10^8, while about 3.4×10^6 events/keV have been collected for the evaluation of the acceptance window efficiency for noise rejection near the software energy threshold [1,6].

The investigation of the DM annual modulation at lower software energy threshold with respect to DAMA/LIBRA–phase1 is deeply supported by the interest in studying the nature of the DM candidate particles, the features of related astrophysical, nuclear and particle physics aspects and by the potentiality of an improved future sensitivity to investigate both DM annual and diurnal signatures.

2.2 The set-up

The full description of the DAMA/LIBRA set-up and the adopted procedures during the phase1 and other related arguments (such as e.g. detector's radiopurity) have been discussed in details e.g. in Ref. [1–5,20] and references therein.

At the end of 2010 the upgrade DAMA/LIBRA–phase2 started. All the photomultipliers (PMTs) were replaced by a second generation PMTs Hamamatsu R6233MOD, with higher quantum efficiency (Q.E.) and with lower background with respect to those used in phase1; they were produced after a dedicated R&D in the company, and tests and selections [6,20]. The new PMTs have Q.E. in the range 33-39% at 420 nm, wavelength of NaI(Tl) emission, and in the range 36-44% at peak. The commissioning of the experiment was successfully performed in 2011, allowing the achievement of the software energy threshold at 1 keV, and the improvement of some detector's features such as energy resolution and acceptance efficiency near software energy threshold[6]; the overall efficiency for *single-hit* events as a function of the energy is also given in Ref. [6]. The procedure adopted in the data analysis has been the same along all the data taking, throughout the months and the annual cycles.

At the end of 2012 new preamplifiers and specially developed trigger modules were installed and the apparatus was equipped with more compact electronic modules [26]. Here we just remind that the sensitive part of DAMA/LIBRA–phase2 set-up is made of 25 highly radio-pure NaI(Tl) crystal scintillators (5-rows by 5-columns matrix) having 9.70 kg mass each one. Quantitative estimates of residual contaminants in the detectors were given in Ref. [1]; the detectors are maintained underground since many years. In each detector two 10 cm long UV light guides (made of Suprasil B quartz) act also as optical windows on the two end faces of the crystal, and are coupled to the two low background high Q.E. PMTs working in coincidence at single photoelectron level. The detectors are housed

in a sealed low-radioactive copper box installed in the center of a multi-ton low-radioactive Cu/Pb/Cd-foils/polyethylene/paraffin shield; moreover, about 1 m concrete (made from the Gran Sasso rock material) almost fully surrounds (mostly outside the barrack) this passive shield, acting as a further neutron moderator. The shield is decoupled from the ground by a metallic structure mounted above a concrete basement; a neoprene layer separates the concrete basement and the floor of the laboratory. The space between this basement and the basis of the metallic structure is filled by paraffin for several tens cm in height.

A threefold-level sealing system prevents the detectors from contact with the environmental air of the underground laboratory and continuously maintains them in HP (high-purity) Nitrogen atmosphere. The whole installation is under air conditioning to ensure a suitable and stable working temperature. The huge heat capacity of the multi-tons passive shield ($\approx 10^6$ cal/°C) guarantees further relevant stability of the detectors' (whose metallic housings are in direct contact with the metallic shield) operating temperature. In particular, two independent systems of air conditioning are available for redundancy: one cooled by water refrigerated by a dedicated chiller and the other operating with cooling gas. A hardware/software monitoring system provides data on the operating conditions. In particular, several probes are read out and the results are stored with the production data. Moreover, self-controlled computer based processes automatically monitor several parameters, including those from DAQ, and manage the alarms system. All these procedures, already experienced during DAMA/LIBRA–phase1 [1–5], allow us to control and to maintain the running conditions stable at a level better than 1% also in DAMA/LIBRA–phase2 (see below).

The light response of the detectors during phase2 typically ranges from 6 to 10 photoelectrons/keV, depending on the detector. Energy calibration with X-rays/γ sources are regularly carried out in the same running condition down to few keV (for details see e.g. Ref. [1]; in particular, double coincidences due to internal X-rays from ^{40}K in trace provide (when summing the data over long periods) an intrinsic calibration point at 3.2 keV, close to the software energy threshold. It is worth noting that, while DAMA/LIBRA–phase1 showed a very good linearity between the calibration with the 59.5 keV line of ^{241}Am and the tagged 3.2 keV line of ^{40}K [1], in DAMA/LIBRA–phase2 a slight non-linearity is observed (it gives a shift of about 0.2 keV at the software energy threshold, as estimated from the tagged 3.2 keV line of ^{40}K, and vanishes above 15 keV which is the position of a bump ascribed to Iodine K-escape peak from small 45 keV structure). This has been taken into account here[1]. It is worth noting that the rates are always already corrected for efficiency and that keV means keV electron equivalent.

The DAQ system records both *single-hit* events (where just one of the detectors fires) and *multiple-hit* events (where more than one detector fires). Data are collected up to the MeV region despite the optimization is performed for the lowest energy range. The duty cycle of the experiment is high, ranging between

[1] Similar non-linear effects cannot be highlighted in experiments where the energy scale is extrapolated from calibrations at much higher energies or estimated through MonteCarlo modeling.

76% and 85%. The routine calibrations and, in particular, the data collection for the acceptance windows efficiency mainly affect it.

The adopted procedures provide sensitivity to large and low mass DM candidates inducing nuclear recoils and/or electromagnetic signals.

2.3 The annual modulation of the residual rate

The analysis of DAMA/LIBRA–phase2 exploits the same procedures already adopted for the DAMA/LIBRA–phase1 [1–5].

In particular, the time behaviour of the experimental residual rates of the *single-hit* scintillation events in the (1–3), and (1–6) keV energy intervals for the DAMA/LIBRA–phase2 is shown in Fig. 2.1. The residual rates are calculated from the measured rate of the *single-hit* events after subtracting the unmodulated part [2–5,16,17]. The null modulation hypothesis is rejected at very high C.L. by χ^2 test: $\chi^2/\mathrm{d.o.f.} = 127.3/52$ and $150.3/52$ (P-values: 3.0×10^{-8} and 1.7×10^{-11}), respectively. We remind that the residuals of the DAMA/NaI data (0.29 ton $\times$ yr) are given in Ref. [2,5,16,17], while those of DAMA/LIBRA–phase1 (1.04 ton $\times$ yr) in Ref. [2–5].

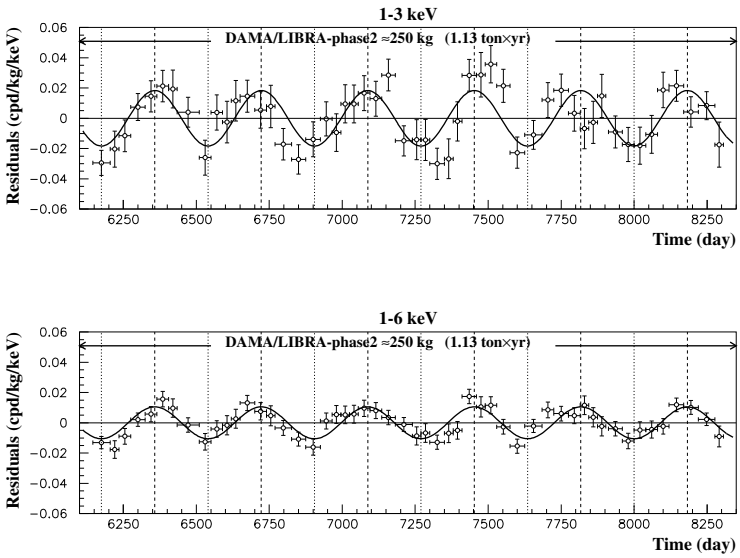

Fig. 2.1. Experimental residual rate of the *single-hit* scintillation events measured by DAMA/LIBRA–phase2 in the (1–3), (1–6) keV energy intervals, respectively, as a function of the time. The time scale is the same as in the previous DAMA data releases for consistency. The data points present the experimental errors as vertical bars, and the widths of the associated time bins as horizontal bars. The superimposed curves are the cosinusoidal functional forms $A\cos\omega(t - t_0)$ with a period $T = \frac{2\pi}{\omega} = 1$ yr, a phase $t_0 = 152.5$ day (June 2^{nd}) and modulation amplitudes, A, equal to the central values obtained by best fit on the data points of the entire DAMA/LIBRA–phase2. The dashed vertical lines correspond to the maximum expected for the DM signal (June 2^{nd}), while the dotted vertical lines correspond to the minimum.

Fig. 2.2 shows the residual rates of the *single-hit* scintillation events of the former DAMA/LIBRA–phase1 and of the new DAMA/LIBRA–phase2; the energy interval is from the software energy threshold of DAMA/LIBRA–phase1 (2keV) up to 6 keV. Again the null modulation hypothesis is rejected at very high C.L. by χ^2 test (χ^2/d.o.f. = 199.3/102, corresponding to P-value = 2.9×10^{-8}).

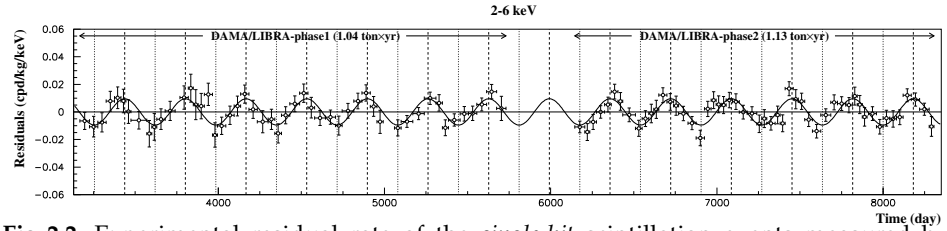

Fig. 2.2. Experimental residual rate of the *single-hit* scintillation events measured by DAMA/LIBRA–phase1 and DAMA/LIBRA–phase2 in the (2–6) keV energy intervals as a function of the time. The superimposed curve is the cosinusoidal functional forms $A \cos \omega(t - t_0)$ with a period $T = \frac{2\pi}{\omega} = 1$ yr, a phase $t_0 = 152.5$ day (June 2^{nd}) and modulation amplitude, A, equal to the central value obtained by best fit on the data points.

The *single-hit* residual rates of the DAMA/LIBRA–phase2 (Fig. 2.1) have been fitted with the function: $A \cos \omega(t - t_0)$, considering a period $T = \frac{2\pi}{\omega} = 1$ yr and a phase $t_0 = 152.5$ day (June 2^{nd}) as expected by the DM annual modulation signature; this can be repeated for the case of (2–6) keV energy interval including also the former DAMA/NaI and DAMA/LIBRA–phase1 data. The goodness of the fits is well supported by the χ^2 test [12]. The results of the fit obtained for DAMA/LIBRA–phase2 either including or not DAMA/NaI and DAMA/LIBRA–phase1 with period and phase kept free in the fitting procedure are reported in Ref. [12]; the obtained period and phase are well compatible with the expectations for a DM annual modulation signal. In particular, the phase is consistent with about June 2^{nd} and is fully consistent with the value independently determined by Maximum Likelihood analysis (see later). For completeness, we recall that a slight energy dependence of the phase could be expected (see e.g. Ref. [24,25,27–30]), providing intriguing information on the nature of the Dark Matter candidate(s) and related aspects.

2.3.1 Absence of background modulation in DAMA/LIBRA-phase2

As done in previous data releases (see e.g. Ref. [5], and references therein), absence of any significant background modulation in the energy spectrum has also been verified in the present data taking for energy regions not of interest for DM. In fact, the background in the lowest energy region is essentially due to "Compton" electrons, X-rays and/or Auger electrons, muon induced events, etc., which are strictly correlated with the events in the higher energy region of the spectrum. Thus, if a modulation detected in the lowest energy region were due to a modulation of the background (rather than to a signal), an equal or larger modulation in the higher energy regions should be present.

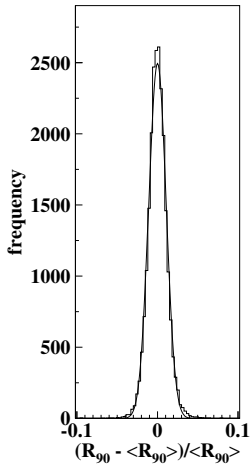

Fig. 2.3. Distribution of the percentage variations of R_{90} with respect to the mean values for all the detectors in DAMA/LIBRA–phase2 (histogram); the superimposed curve is a gaussian fit. See text.

For example, the measured rate integrated above 90 keV, R_{90}, as a function of the time has been analysed. Fig. 2.3 shows the distribution of the percentage variations of R_{90} with respect to the mean values for all the detectors in DAMA/LIBRA–phase2; this has a cumulative gaussian behaviour with $\sigma \simeq 1\%$, well accounted by the statistical spread expected from the used sampling time. Moreover, fitting the time behaviour of R_{90} including also a term with phase and period as for DM particles, a modulation amplitude $A_{R_{90}}$ compatible with zero has been found for all the annual cycles (see Ref. [12]). This also excludes the presence of any background modulation in the whole energy spectrum at a level much lower than the effect found in the lowest energy range for the *single-hit* scintillation events. In fact, otherwise – considering the R_{90} mean values – a modulation amplitude of order of tens cpd/kg would be present for each annual cycle, that is $\simeq 100\ \sigma$ far away from the measured values. Similar results are obtained when comparing the *single-hit* residuals in the (1–6) keV with those in other energy intervals [12].

A further relevant investigation on DAMA/LIBRA–phase2 data has been performed by applying the same hardware and software procedures, used to acquire and to analyse the *single-hit* residual rate, to the *multiple-hit* one. Since the probability that a DM particle interacts in more than one detector is negligible, a DM signal can be present just in the *single-hit* residual rate. Thus, the comparison of *single-hit* events with *multiple-hit* events corresponds to compare the cases of DM particles beam-on and beam-off. This procedure also allows an additional test of the background behaviour in the same energy interval where the positive effect is observed. We note that an event is considered *multiple-hit* when there is a deposition of energy in coincidence in more than one detector of the set-up. The multiplicity can, in principle, range from 2 to 25. A *multiple-hit* event in a given energy interval, say (1–6) keV, is given by an energy deposition between 1 and 6

keV in one detector and other deposition(s) in other detector(s). The residual rate of events with multiplicity equal or greater than 2 with an energy deposition in the range 1-6 keV is shown in Fig. 2.4; the only procedure applied to *multiple-hit* events is that used to reject noise events near software energy threshold and is the same used for *single-hit* events. In particular, in Fig. 2.4 the residual rates of the

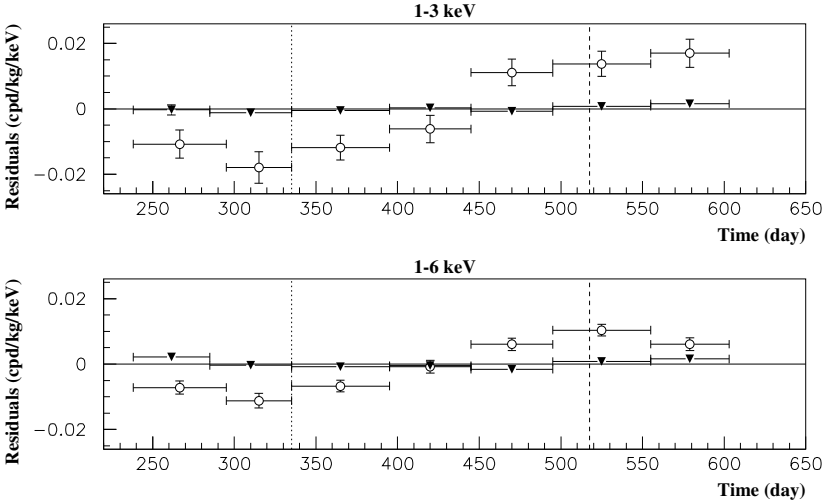

Fig. 2.4. Experimental residual rates of DAMA/LIBRA–phase2 *single-hit* events (open circles), class of events to which DM events belong, and for *multiple-hit* events (filled triangles), class of events to which DM events do not belong. They have been obtained by considering for each class of events the data as collected in a single annual cycle and by using in both cases the same identical hardware and the same identical software procedures. The initial time of the figure is taken on August $7^{\rm th}$. The experimental points present the errors as vertical bars and the associated time bin width as horizontal bars. Analogous results were obtained for DAMA/NaI (two last annual cycles) and DAMA/LIBRA–phase1 [2–5,17,10].

single-hit scintillation events collected during DAMA/LIBRA–phase2 are reported, as collected in a single cycle, together with the residual rates of the *multiple-hit* events, in the considered energy intervals[2]. While, as already observed, a clear modulation, satisfying all the peculiarities of the DM annual modulation signature, is present in the *single-hit* events, the fitted modulation amplitudes for the *multiple-hit* residual rate are well compatible with zero: (0.0007 ± 0.0006) cpd/kg/keV, and (0.0004 ± 0.0004) cpd/kg/keV, in the energy regions (1–3) keV, and (1–6) keV, respectively. Thus, again evidence of annual modulation with proper features as required by the DM annual modulation signature is present in the *single-hit* residuals (events class to which the DM particle induced events belong), while it is absent in the *multiple-hit* residual rate (event class to which only background events belong). Similar results were also obtained for the two last annual cycles of DAMA/NaI [17] and for DAMA/LIBRA–phase1 [2–5]. Since the same identical

[2] Just for completeness, it is worth noting that the rate of the *multiple-hit* events is $\lesssim 0.1$ cpd/kg/keV and is dominated by double hit events from residual ^{40}K in the crystals.

hardware and the same identical software procedures have been used to analyse the two classes of events, the obtained result offers an additional support for the presence of a DM particle component in the galactic halo.

In conclusion, no background process able to mimic the DM annual modulation signature (that is, able to simultaneously satisfy all the peculiarities of the signature and to account for the measured modulation amplitude) has been found or suggested by anyone throughout some decades thus far (see also discussions e.g. in Ref. [1–5,7,8,10]).

2.3.2 The analysis in frequency

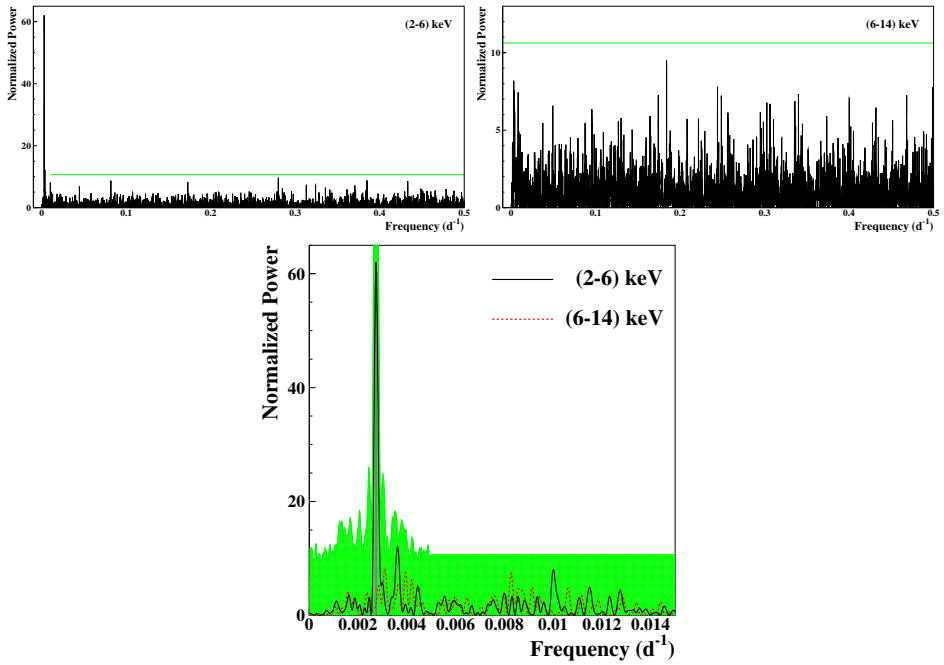

Fig. 2.5. Power spectra of the time sequence of the measured *single-hit* events for DAMA/LIBRA–phase1 and DAMA/LIBRA–phase2 grouped in 1 day bins. From top to bottom: spectra up to the Nyquist frequency for (2–6) keV and (6–14) keV energy intervals and their zoom around the 1 y^{-1} peak, for (2–6) keV (solid line) and (6–14) keV (dotted line) energy intervals. The main mode present at the lowest energy interval corresponds to a frequency of 2.74×10^{-3} d^{-1} (vertical line, purple on-line). It corresponds to a period of $\simeq 1$ year. A similar peak is not present in the (6–14) keV energy interval. The shaded (green on-line) area in the bottom figure – calculated by Monte Carlo procedure – represents the 90% C.L. region where all the peaks are expected to fall for the (2–6) keV energy interval. In the frequency range far from the signal for the (2–6) keV energy region and for the whole (6–14) keV spectrum, the upper limit of the shaded region (90% C.L.) can be calculated to be 10.6 (continuous lines, green on-line).

To perform the Fourier analysis of the DAMA/LIBRA–phase1 and –phase2 data in a wider region of considered frequency, the *single-hit* events have been

grouped in 1 day bins. Because of the low statistics in each time bin, a procedure described in Ref. [31] has been followed. The whole power spectra up to the Nyquist frequency and the zoomed ones are reported in Fig. 2.5. For the lowest energy interval a clear peak corresponding to a period of 1 year is evident, while in the (6–14) keV energy region the same analysis gives only aliasing peaks. Neither other structure at different frequencies has been observed.

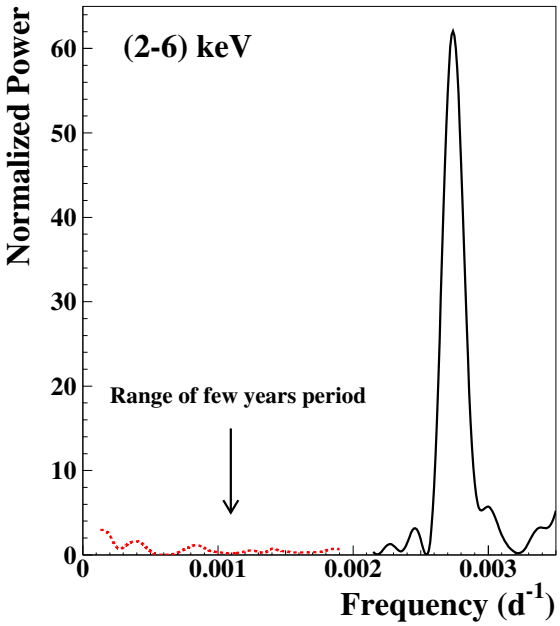

Fig. 2.6. Power spectrum of the annual baseline counting rates for the *single-hit* events of DAMA/LIBRA–phase1 and DAMA/LIBRA–phase2 in the (2–6) keV energy interval (dotted line, red on-line). Also shown for comparison is the power spectrum reported in Fig. 2.5 (solid line). The calculation has been performed according to Ref. [5]. As can be seen, a principal mode is present at a frequency of 2.74×10^{-3} d^{-1}, that corresponds to a period of $\simeq 1$ year. No statistically-significant peak is present at lower frequencies. This implies that no evidence for a long term modulation is present in the *single-hit* scintillation event in the low energy range.

As regards the significance of the peaks present in the periodogram, we remind that the periodogram ordinate, z, at each frequency follows a simple exponential distribution e^{-z} in the case of the null hypothesis or white noise [32]. Thus, if M independent frequencies are scanned, the probability to obtain values larger than z is: $P(> z) = 1 - (1 - e^{-z})^M$; in general M depends on the number of sampled frequencies, the number of data points N, and their detailed spacing. It turns out that M is very nearly equal to N when the data points are approximately equally spaced, and when the sampled frequencies cover the frequency range from 0 to the Nyquist frequency [33,34].

The number of data points used to obtain the spectra in Fig. 2.5 is N = 4341 (days measured over the 4748 days of the 13 DAMA/LIBRA–phase1 and

–phase2 annual cycles) and the full frequencies region up to Nyquist frequency has been scanned. Therefore, assuming $M = N$, the significance levels $P = 0.10$, 0.05 and 0.01, correspond to peaks with heights larger than $z = 10.6$, 11.3 and 13.0, respectively, in the spectra of Fig 2.5.

In the case below 6 keV, a signal is present; thus, the signal must be included to properly evaluate the C.L.. This has been done by a dedicated Monte Carlo procedure where a large number of similar experiments has been simulated. The 90% C.L. region (shaded, green on-line) where all the peaks are expected to fall for the (2–6) keV energy interval is shown in Fig 2.5; several peaks, satellite of the one year period frequency, are present.

The case of the (1–6) keV energy interval can be studied only for DAMA/LIBRA–phase2 and is shown in Ref. [12]; as previously, the only significant peak is that corresponding to one year period. No other peak is statistically significant being below the area obtained by Monte Carlo procedure.

In conclusion, apart from the peak corresponding to a 1 year period, no other peak is statistically significant either in the low and in the high energy regions.

In addition, for each annual cycle of DAMA/LIBRA–phase1 and –phase2, the annual baseline counting rates have been calculated for the (2–6) keV energy interval. Their power spectrum in the frequency range $0.0002 - 0.0018$ d^{-1} (corresponding to a period range 13.7–1.5 year) is reported in Fig. 2.6; for comparison the power spectrum (solid black line) above 0.0022 d^{-1} of Fig. 2.5 is shown. The calculation has been performed according to Ref. [5]. No statistically-significant peak is present at frequencies lower than 1 y^{-1}. This implies that no evidence for a long term modulation in the counting rate is present.

2.4 The modulation amplitudes by maximum likelihood approach

The annual modulation present at low energy can also be pointed out by depicting the energy dependence of the modulation amplitude, $S_m(E)$, obtained by maximum likelihood method considering fixed period and phase: $T = 1$ yr and $t_0 = 152.5$ day. For such purpose the likelihood function of the *single-hit* experimental data in the $k-$th energy bin is defined as:

$$\mathbf{L_k} = \Pi_{ij} e^{-\mu_{ijk}} \frac{\mu_{ijk}^{N_{ijk}}}{N_{ijk}!} , \tag{2.1}$$

where N_{ijk} is the number of events collected in the i-th time interval (hereafter 1 day), by the j-th detector and in the k-th energy bin. N_{ijk} follows a Poisson's distribution with expectation value:

$$\mu_{ijk} = [b_{jk} + S_i(E_k)] M_j \Delta t_i \Delta E \epsilon_{jk} . \tag{2.2}$$

The b_{jk} are the time-independent background contributions that depend on the energy and on the detector, M_j is the mass of the $j-$th detector, Δt_i is the detector running time during the i-th time interval, ΔE is the chosen energy bin, ϵ_{jk} is the overall efficiency.

The signal can be written as:

$$S_i(E) = S_0(E) + S_m(E) \cdot \cos\omega(t_i - t_0)\ , \tag{2.3}$$

where $S_0(E)$ is the constant part of the signal and $S_m(E)$ is the modulation amplitude. The usual procedure is to minimize the function $y_k = -2\ln(\mathbf{L_k}) - const$ for each energy bin; the free parameters of the fit are the twenty-five (one for each detector) $f_{jk} = (b_{jk} + S_0)$ contributions and the S_m parameter.

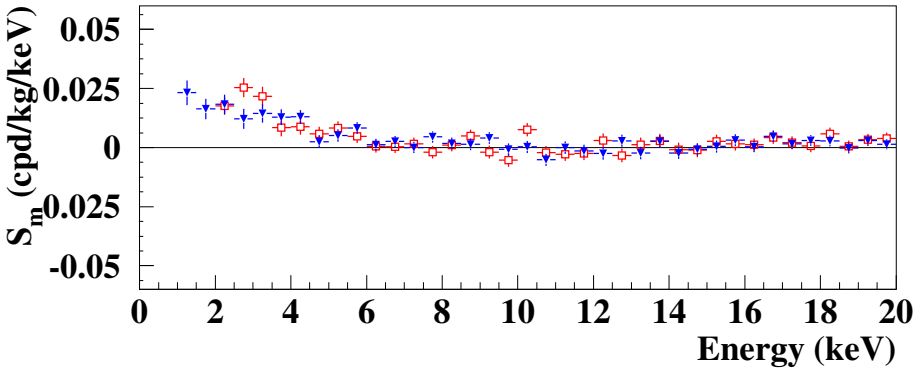

Fig. 2.7. Modulation amplitudes, S_m, for DAMA/LIBRA–phase2 (exposure 1.13 ton×yr) from the energy threshold of 1 keV up to 20 keV (full triangles, blue data points on-line) – and for DAMA/NaI and DAMA/LIBRA–phase1 (exposure 1.33 ton×yr) [4] (open squares, red data points on-line). The energy bin ΔE is 0.5 keV. The modulation amplitudes obtained in the two data sets are consistent in the (2–20) keV: the χ^2 is 32.7 for 36 d.o.f., and the corresponding P-value is 63%. In the (2–6) keV energy region, where the signal is present, the χ^2/d.o.f. is 10.7/8 (P-value = 22%).

The modulation amplitudes obtained considering the DAMA/LIBRA–phase2 data are reported in Fig. 2.7 as full triangles (blue points on-line) from the energy threshold of 1 keV up to 20 keV; superimposed to the picture as open squared (red on-line) data points are the modulation amplitudes of the former DAMA/NaI and DAMA/LIBRA–phase1 [4]. The modulation amplitudes obtained in the two data sets are consistent in the (2–20) keV, since the χ^2 is 32.7 for 36 d.o.f. corresponding to P-value = 63%. In the (2–6) keV energy region, where the signal is present, the χ^2/d.o.f. is 10.7/8 (P-value = 22%).

As shown in Fig. 2.7 positive signal is present below 6 keV also in the case of DAMA/LIBRA–phase2. Above 6 keV the S_m values are compatible with zero; actually, they have random fluctuations around zero, since the χ^2 in the (6–20) keV energy interval for the DAMA/LIBRA–phase2 data is equal to 29.8 for 28 d.o.f. (upper tail probability of 37%). Similar considerations have been done for DAMA/NaI and DAMA/LIBRA–phase1 where the χ^2 in the (6–20) keV energy interval is 35.8 for 28 d.o.f. (upper tail probability of 15%) [4].

The modulation amplitudes for the whole data sets: DAMA/NaI, DAMA/LIBRA–phase1 and DAMA/LIBRA–phase2 are plotted in Fig. 2.8; the data below 2 keV refer only to DAMA/LIBRA–phase2. It can be inferred that positive signal

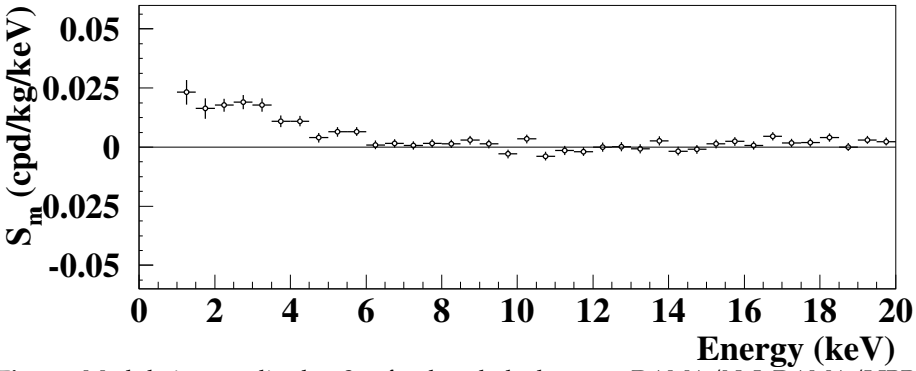

Fig. 2.8. Modulation amplitudes, S_m, for the whole data sets: DAMA/NaI, DAMA/LIBRA–phase1 and DAMA/LIBRA–phase2 (total exposure 2.46 ton×yr) above 2 keV; below 2 keV only the DAMA/LIBRA–phase2 exposure (1.13 ton × yr) is available and used. The energy bin ΔE is 0.5 keV. A clear modulation is present in the lowest energy region, while S_m values compatible with zero are present just above. In fact, the S_m values in the (6–20) keV energy interval have random fluctuations around zero with χ^2 equal to 42.6 for 28 d.o.f. (upper tail probability of 4%); see text for comments.

is present in the (1–6) keV energy interval, while S_m values compatible with zero are present just above. All this confirms the previous analyses. The test of the hypothesis that the S_m values in the (6–14) keV energy interval have random fluctuations around zero yields χ^2 equal to 19.0 for 16 d.o.f. (upper tail probability of 27%).

For the case of (6–20) keV energy interval $\chi^2/\text{d.o.f.} = 42.6/28$ (upper tail probability of 4%). The obtained χ^2 value is rather large due mainly to two data points, whose centroids are at 16.75 and 18.25 keV, far away from the (1–6) keV energy interval. The P-values obtained by excluding only the first and either the points are 11% and 25%.

2.4.1 The S_m distributions

The S_m values for each detector in the energy intervals of interest can be obtained by the maximum likelihood approach. In particular, Fig. 2.9 shows the modulation amplitudes S_m in the range (2–6) keV for each one of the 25 detectors in the DAMA/LIBRA–phase1 and DAMA/LIBRA–phase2 periods. The hypothesis that the signal is well distributed over all the 25 detectors is supported by the χ^2 analysis; in fact, the S_m values show a random behaviour around the weighted averaged value (shaded band), and the $\chi^2/\text{d.o.f.}$ is 23.9/24.

The S_m values for each detector for each annual cycle and for the energy bin of interest are expected to follow a normal distribution in absence of systematic effects. One can consider the variable $x = \frac{S_m - \langle S_m \rangle}{\sigma}$ in each detector, in 16 energy bins ($\Delta E = 0.25$ keV) in the (2–6) keV energy interval, for the seven DAMA/LIBRA–phase1 annual cycles and in the 20 energy bins in the (1–6) keV energy interval for the six DAMA/LIBRA–phase2 annual cycles. The errors associated to S_m are σ and $\langle S_m \rangle$ are the mean values of the S_m averaged over the detectors and the

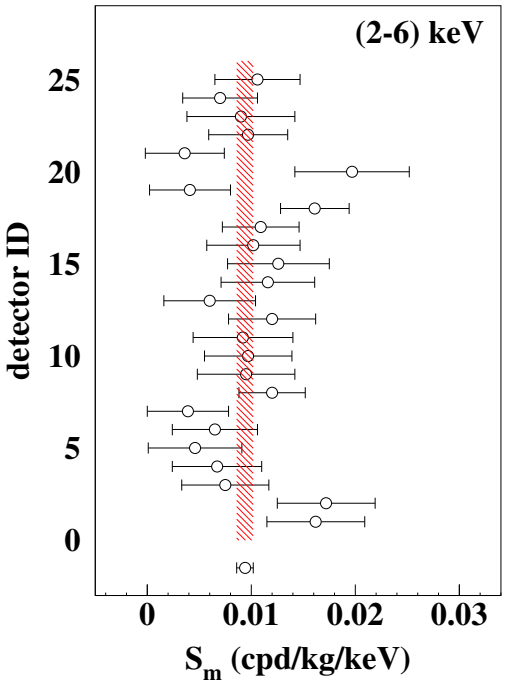

Fig. 2.9. Modulation amplitudes S_m integrated in the range (2–6) keV for each of the 25 detectors for the DAMA/LIBRA–phase1 and DAMA/LIBRA–phase2 periods. The errors are at 1σ confidence level. The weighted averaged point and 1σ band (shaded area) are also reported. The χ^2 is 23.9 over 24 d.o.f., supporting the hypothesis that the signal is well distributed over all the 25 detectors.

annual cycles for each considered energy bin. Fig. 2.10 shows the x distributions and the gaussian fits.

Defining $\chi^2 = \Sigma x^2$, where the sum is extended over all the 232 (152 for the 16^{th} detector [4]), χ^2/d.o.f. values ranging from 0.69 to 1.95 are obtained for the 25 detectors. The mean value of χ^2/d.o.f. is 1.07, value slightly larger than 1; this can be still ascribed to statistical fluctuations, anyhow in case one would assume it as ascribed to systematics an additional error to the modulation amplitude measured below 6 keV would be derived as: $\leq 2.1 \times 10^{-4}$ cpd/kg/keV, if combining quadratically the errors, or $\leq 3.0 \times 10^{-5}$ cpd/kg/keV, if linearly combining them. This possible additional error: $\leq$ 2% or $\leq$ 0.3%, respectively, on the DAMA/LIBRA–phase1 and DAMA/LIBRA–phase2 modulation amplitudes is an upper limit of possible systematic effects.

The analysis of the energy behaviour of the modulation amplitudes obtained considering the nine inner detectors and the remaining external ones has also been carried out for DAMA/LIBRA–phase2 as already done for the other data sets. The hypothesis that the two sets of modulation amplitudes as a function of the energy belong to same distribution has been verified by χ^2 test, obtaining e.g.: χ^2/d.o.f. = 2.5/6 and 40.8/38 for the energy intervals (1–4) and (1–20) keV, respectively (ΔE

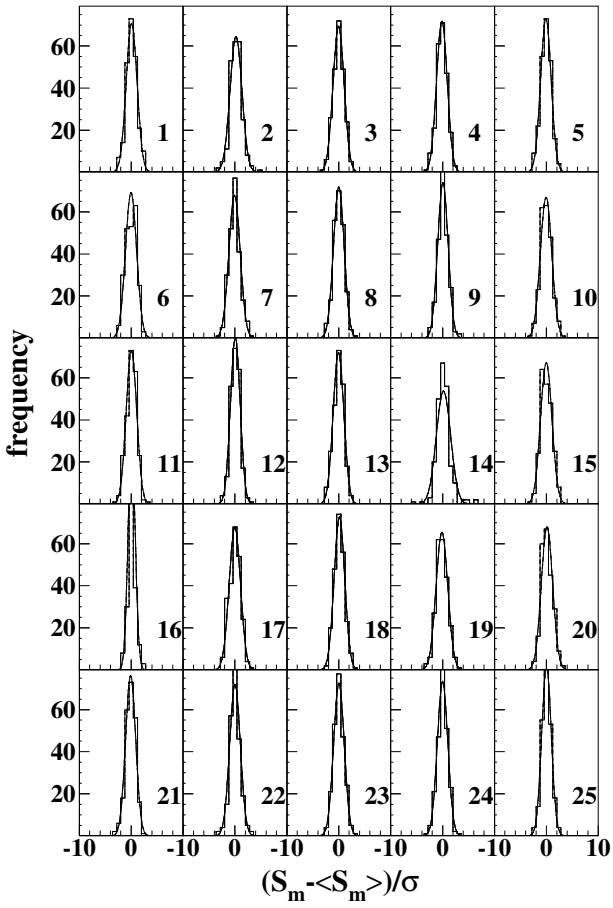

Fig. 2.10. Histograms of the variable $\frac{S_m - \langle S_m \rangle}{\sigma}$, where σ are the errors associated to the S_m values and $\langle S_m \rangle$ are the mean values of the modulation amplitudes averaged over the detectors and the annual cycles for each considered energy bin (here $\Delta E = 0.25$ keV). Each panel refers to a single DAMA/LIBRA detector. The entries of each histogram are 232 (the 16 energy bins in the (2–6) keV energy interval of the seven DAMA/LIBRA–phase1 annual cycles and the 20 energy bins in the (1–6) keV energy interval of the six DAMA/LIBRA–phase2 annual cycles), but 152 for the 16^{th} detector (see Ref. [4]). The superimposed curves are gaussian fits.

= 0.5 keV). Thus it is possible to conclude that the effect is well shared between internal and external detectors.

To evaluate the hypothesis that the modulation amplitudes obtained for each annual cycle are compatible and normally fluctuating around their mean values a χ^2 test can be applied. The distribution of these modulation amplitudes are reported in Fig. 2.11, where the $\chi^2/d.o.f.$ are also given; they corresponds to upper tail probability of 5.2%, 97%, 25%, 67% and 72%, respectively. In addition to the χ^2 test, also the *run test* has been applied (see e.g. Ref. [35]); it verifies the hypothesis

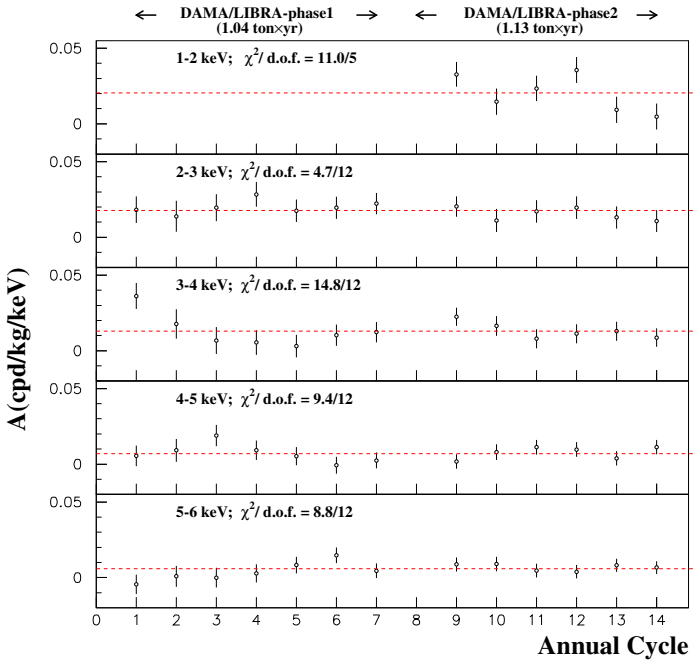

Fig. 2.11. Modulation amplitudes of each single annual cycle of DAMA/LIBRA–phase1 and DAMA/LIBRA–phase2. The error bars are the 1σ errors. The dashed horizontal lines show the central values obtained by best fit over the whole data set. The χ^2 test and the *run test* accept the hypothesis at 95% C.L. that the modulation amplitudes are normally fluctuating around the best fit values.

that the positive (above the mean value) and negative (under the mean value) data points are randomly distributed. The lower (upper) tail probabilities obtained by the *run test* are: 70(70)%, 50(73)%, 85(35)%, 88(30)% and 88(30)%, respectively; this confirms that the data collected in all the annual cycles with DAMA/LIBRA–phase1 and phase2 are statistically compatible and can be considered together.

2.5 The phase of the measured modulation effect

In order to investigate the phase of the annual modulation effect, it is useful to write the the signal as:

$$\begin{aligned} S_i(E) &= S_0(E) + S_m(E)\cos\omega(t_i - t_0) + Z_m(E)\sin\omega(t_i - t_0) \\ &= S_0(E) + Y_m(E)\cos\omega(t_i - t^*) \end{aligned} \tag{2.4}$$

releasing the assumption of a fixed phase at $t_0 = 152.5$ day. For DM induced signals: i) $Z_m \sim 0$ (because of the orthogonality between the cosine and the sine functions); ii) $S_m \simeq Y_m$; iii) $t^* \simeq t_0 = 152.5$ day. In fact, these conditions hold for most of the dark halo models with some exceptions (see e.g. Ref. [24,25,27–30]).

In Fig. 2.12–*left* the obtained 2σ contours in the plane (S_m, Z_m) are shown for the (2–6) keV and (6–14) keV energy intervals considering cumulatively the data

of DAMA/NaI, DAMA/LIBRA–phase1 and DAMA/LIBRA–phase2. In Fig. 2.12–*right* instead the obtained 2σ contours in the plane (Y_m, t^*) are depicted. Fig. 2.12 also shows – obviously only for DAMA/LIBRA–phase2 – the 2σ contours in the (1–6) keV energy interval.

The best fit values in the considered cases (1σ errors) for S_m versus Z_m and Y_m versus t^* are reported in Table 2.1.

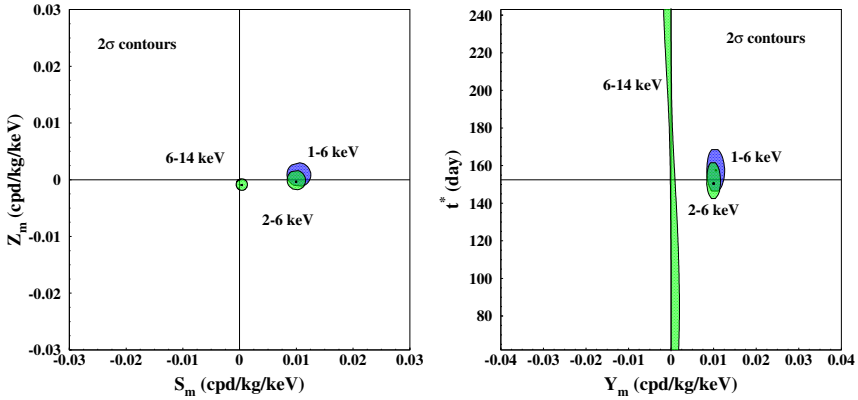

Fig. 2.12. 2σ contours in the plane (S_m, Z_m) (*left*) and in the plane (Y_m, t^*) (*right*) for: i) DAMA/NaI, DAMA/LIBRA–phase1 and DAMA/LIBRA–phase2 in the (2–6) keV and (6–14) keV energy intervals (light areas, green on-line); ii) only DAMA/LIBRA–phase2 in the (1–6) keV energy interval (dark areas, blue on-line). The contours have been obtained by the maximum likelihood method. A modulation amplitude is present in the lower energy intervals and the phase agrees with that expected for DM induced signals.

E (keV)	S_m (cpd/kg/keV)	Z_m (cpd/kg/keV)	Y_m (cpd/kg/keV)	t^* (day)
DAMA/NaI+DAMA/LIBRA–phase1+DAMA/LIBRA–phase2:				
2–6	(0.0100 ± 0.0008)	$-(0.0003 \pm 0.0008)$	(0.0100 ± 0.0008)	(150.5 ± 5.0)
6–14	(0.0003 ± 0.0005)	$-(0.0009 \pm 0.0006)$	(0.0010 ± 0.0013)	undefined
DAMA/LIBRA–phase2:				
1–6	(0.0105 ± 0.0011)	(0.0009 ± 0.0010)	(0.0105 ± 0.0011)	(157.5 ± 5.0)

Table 2.1. Best fit values (1σ errors) for S_m versus Z_m and Y_m versus t^*, considering: i) DAMA/NaI, DAMA/LIBRA–phase1 and DAMA/LIBRA–phase2 in the (2–6) keV and (6–14) keV energy intervals; ii) only DAMA/LIBRA–phase2 in the (1–6) keV energy interval. See also Fig. 2.12.

The Z_m values, obtained in the hypothesis of S_m set to zero in eq. (2.4), are reported in Fig. 2.13 for DAMA/NaI, DAMA/LIBRA–phase1, and DAMA/LIBRA–phase2; they are expected to be zero. The χ^2 test of the data supports the hypothesis

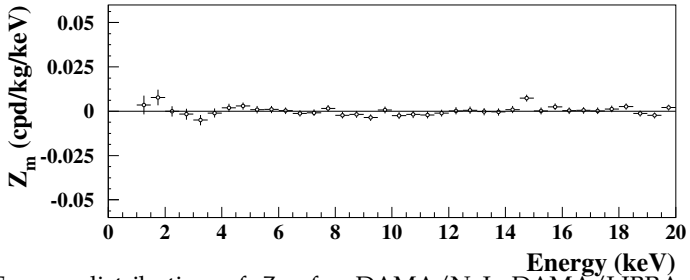

Fig. 2.13. Energy distribution of Z_m for DAMA/NaI, DAMA/LIBRA–phase1, and DAMA/LIBRA–phase2 once setting S_m in eq. (2.4) to zero. The energy bin ΔE is 0.5 keV. The χ^2 test applied to the data supports the hypothesis that the Z_m values are simply fluctuating around zero, as expected. See text.

that the Z_m values are simply fluctuating around zero; in fact, in the (1–20) keV energy region the χ^2/d.o.f. is equal to 44.5/38 corresponding to a P-value = 22%.

Fig. 2.14 shows Y_m and t^* as a function of the energy for DAMA/NaI, DAMA/LIBRA–phase1, and DAMA/LIBRA–phase2. The Y_m are superimposed with the S_m values with 1 keV energy bin. As in the previous analyses, an annual modulation effect is present in the lower energy intervals and the phase agrees with that expected for DM induced signals. No modulation is present above 6 keV and the phase is undetermined.

2.6 Further investigation on possible systematic effects and side reactions in DAMA/LIBRA–phase2

The DAMA/LIBRA–phase2 results – as those of DAMA/LIBRA–phase1 and DAMA/NaI – fulfill the requirements of the DM annual modulation signature and investigations on absence of any significant systematics or side reaction effect are already present in the previous sections; however, here the topic is further addressed.

Sometimes naive statements are put forwards as the fact that in nature several phenomena may show annual periodicity. However, the point is whether they might mimic the annual modulation signature, i.e. whether they might be not only able to quantitatively account for the observed modulation amplitude but also to contemporaneously satisfy all the requirements of the DM annual modulation signature. This was deeply investigated in the former DAMA/NaI and DAMA/LIBRA–phase1 experiments (see e.g. Ref. [16,17,2] and references therein; no one able to mimic the signature has been found or suggested by anyone so far) and will be further addressed in the following for the present DAMA/LIBRA–phase2 data.

Firstly, in order to continuously monitor the running conditions, several pieces of information are acquired with the production data and quantitatively analysed; information on technical aspects of DAMA/LIBRA has been given in Ref. [1], where the sources of possible residual radioactivity have also been analysed.

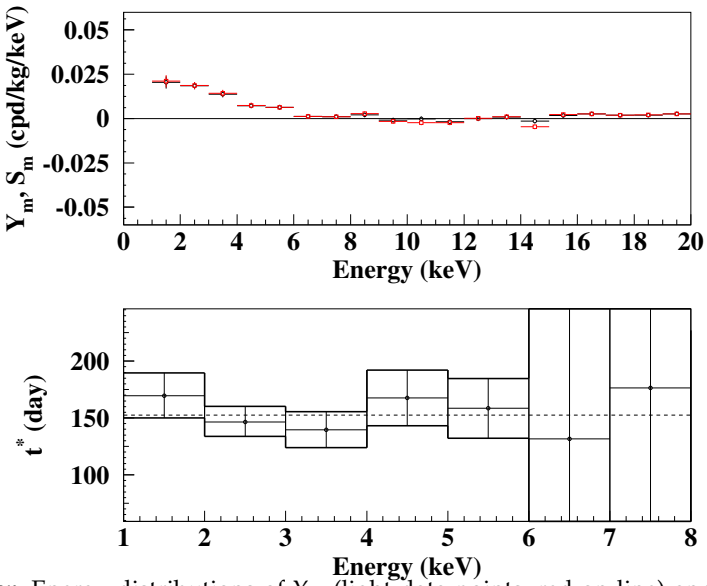

Fig. 2.14. *Top:* Energy distributions of Y_m (light data points; red on-line) and of the S_m variable (solid data points; black on-line) for DAMA/NaI, DAMA/LIBRA–phase1, and DAMA/LIBRA–phase2. Here, unlike the data of Fig. 2.8, the energy bin is 1 keV. *Bottom:* Energy distribution of the phase t^* for DAMA/NaI, DAMA/LIBRA–phase1, and DAMA/LIBRA–phase2; here the errors are at 2σ. The vertical scale spans over $\pm$ a quarter of period around 2 June; other intervals are replica of it. The phase agrees with that expected for DM induced signals at low energy. No modulation is present above 6 keV and thus the phase is undetermined.

	LIBRA–phase2-2	LIBRA–phase2-3	LIBRA–phase2-4	LIBRA–phase2-5	LIBRA–phase2-6	LIBRA–phase2-7
Temperature (°C)	(0.0012 ± 0.0051)	$-(0.0002 \pm 0.0049)$	$-(0.0003 \pm 0.0031)$	(0.0009 ± 0.0050)	(0.0018 ± 0.0036)	$-(0.0006 \pm 0.0035)$
Flux (l/h)	$-(0.15 \pm 0.18)$	$-(0.02 \pm 0.22)$	$-(0.02 \pm 0.12)$	$-(0.02 \pm 0.14)$	$-(0.01 \pm 0.10)$	$-(0.01 \pm 0.16)$
Pressure (mbar)	$(1.1 \pm 0.9)10^{-3}$	$(0.2 \pm 1.1)10^{-3}$	$(2.4 \pm 5.4)10^{-3}$	$(0.6 \pm 6.2)10^{-3}$	$(1.5 \pm 6.3)10^{-3}$	$(7.2 \pm 8.6)10^{-3}$
Radon (Bq/m^3)	(0.015 ± 0.034)	$-(0.002 \pm 0.050)$	$-(0.009 \pm 0.028)$	$-(0.044 \pm 0.050)$	(0.082 ± 0.086)	(0.06 ± 0.11)
Hardware rate (Hz)	$-(0.12 \pm 0.16)10^{-2}$	$(0.00 \pm 0.12)10^{-2}$	$-(0.14 \pm 0.22)10^{-2}$	$-(0.05 \pm 0.22)10^{-2}$	$-(0.06 \pm 0.16)10^{-2}$	$-(0.08 \pm 0.17)10^{-2}$

Table 2.2. Modulation amplitudes (1 σ error) obtained – for each annual cycle – by fitting the time behaviours of main running parameters including a possible annual modulation with phase and period as for DM particles. These running parameters, acquired with the production data, are: i) the operating temperature of the detectors; ii) the HP Nitrogen flux in the inner Cu box housing the detectors; iii) the pressure of the HP Nitrogen atmosphere of that inner Cu box; iv) the environmental Radon in the inner part of the barrack from which the detectors are however excluded by other two sealing systems (see text and Ref. [1] for details); v) the hardware rate above single photoelectron threshold. All the measured amplitudes are compatible with zero.

In particular, all the time behaviours of the running parameters, acquired with the production data, have been investigated. Table 2.2 shows the modulation

amplitudes obtained for each annual cycle when fitting the time behaviours of the values of the main parameters including a cosine modulation with the same phase and period as for DM particles. As can be seen, all the measured amplitudes are well compatible with zero.

Let us now enter in some more details.

2.6.1 The temperature

The full experiment is placed underground and works in an air-conditioned environment; moreover, the detectors have Cu housing in direct contact with the multi-tons metallic passive shield whose huge heat capacity definitively assures a relevant stability of the detectors' operating temperature [1]. Nevertheless the operating temperature is read out by a probe and stored with the production data, in order to offer the possibility of further investigations.

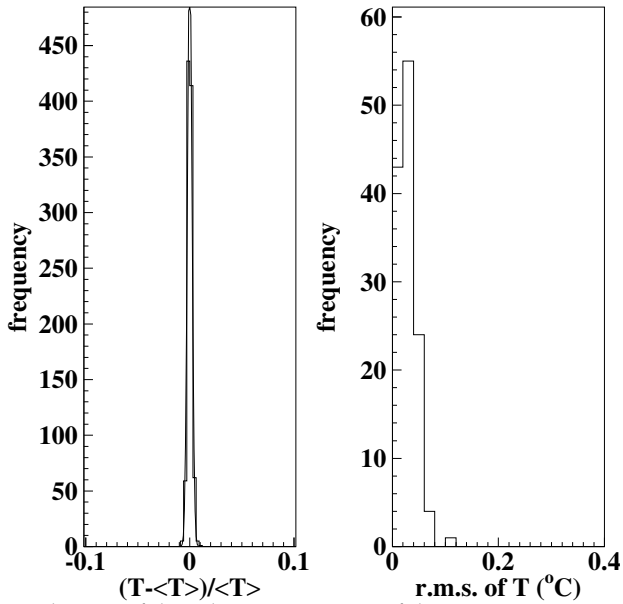

Fig. 2.15. *left* - Distribution of the relative variations of the operating temperature measured during the DAMA/LIBRA–phase2 six annual cycles (histogram); the superimposed curve is a gaussian fit. The standard deviation is 0.2%. *Right* - Distribution of the root mean square (r.m.s.) detectors' operating temperature variations within periods with the same calibration factors (typically $\simeq$ 10 days) during the DAMA/LIBRA–phase2 six annual cycles. The mean value is 0.03 ^{o}C.

Specific information on the DAMA/LIBRA–phase2 six annual cycles can be derived from Fig. 2.15-*left*; no evidence for any operating temperature modulation has been observed, as also quantitatively reported in Table 2.2. However, to properly evaluate the real effect of possible variations of the detectors' operating temperature on the light output, we consider the distribution of the root mean square temperature variations within periods with the same calibration factors (typically $\simeq$ 10 days); this is given in Fig. 2.15-*right* cumulatively for the

DAMA/LIBRA–phase2 data. The mean value of the root mean square of the variation of the detectors' operating temperature is $\simeq 0.03$ °C and, considering the known value of the slope of the light output $\lesssim$-0.2%/°C, the relative light output variation is $\lesssim 10^{-4}$, that would correspond to a modulation amplitude $\lesssim 10^{-4}$ cpd/kg/keV (that is $\lesssim$0.5% of the observed modulation amplitude).

Moreover, for temperature variations the specific requirements of the DM annual modulation signature (such as e.g. the 4^{th} and the 5^{th}) would fail, while they are instead satisfied by the DAMA/LIBRA–phase2 production data.

In conclusion, all the arguments given above quantitatively exclude any role of possible effects on the observed rate modulation directly correlated with temperature.

For the sake of completeness, we comment that sizeable temperature variations in principle might also induce variations in the electronic noise, in the Radon release from the rocks and in some environmental background; these specific topics will be further addressed in the following.

2.6.2 The noise

Despite the good noise identification near energy threshold and the stringent noise rejection procedure which is used [1,6], the role of a possible noise tail in the data after the noise rejection procedure has been quantitatively investigated.

The hardware rate of each detector above a single photoelectron, R_{Hj} (j identifies the detector), has been considered. Indeed, this hardware rate is significantly determined by the noise.

For the proposed purpose the variable: $R_H = \Sigma_j(R_{Hj} - \langle R_{Hj}\rangle)$, can be built; in the present case $\langle R_{Hj}\rangle \lesssim 0.2$ Hz. The time behaviour of R_H during each DAMA/LIBRA–phase2 annual cycle is shown in Fig. 2.16. As can be seen in Fig. 2.17, the cumulative distribution of R_H for the DAMA/LIBRA–phase2 annual cycles shows a gaussian behaviour with σ = 0.3%, that is well in agreement with that expected on the basis of simple statistical arguments.

Moreover, by fitting the time behaviour of R_H in the six data taking periods – including a modulation term as that for DM particles – a modulation amplitude compatible with zero is obtained: $-(0.061 \pm 0.067) \times 10^{-2}$ Hz, corresponding to the upper limit: $< 0.6 \times 10^{-3}$ Hz at 90% C.L.. Since the typical noise contribution to the hardware rate of each detector is $\simeq 0.10$ Hz, the upper limit on the noise relative modulation amplitude is given by: $\frac{0.6\times10^{-3}\,\mathrm{Hz}}{2.5\mathrm{Hz}} \simeq 2.4 \times 10^{-4}$ (90% C.L.). Therefore, even in the worst hypothetical case of a 10% contamination of the residual noise – after rejection – in the counting rate, the noise contribution to the modulation amplitude in the lowest energy bins would be $< 2.4 \times 10^{-5}$ of the total counting rate. This means that a hypothetical noise modulation could account at maximum for absolute amplitudes less than 10^{-4} cpd/kg/keV.

In conclusion, there is no role of any hypothetical tail of residual noise after rejection.

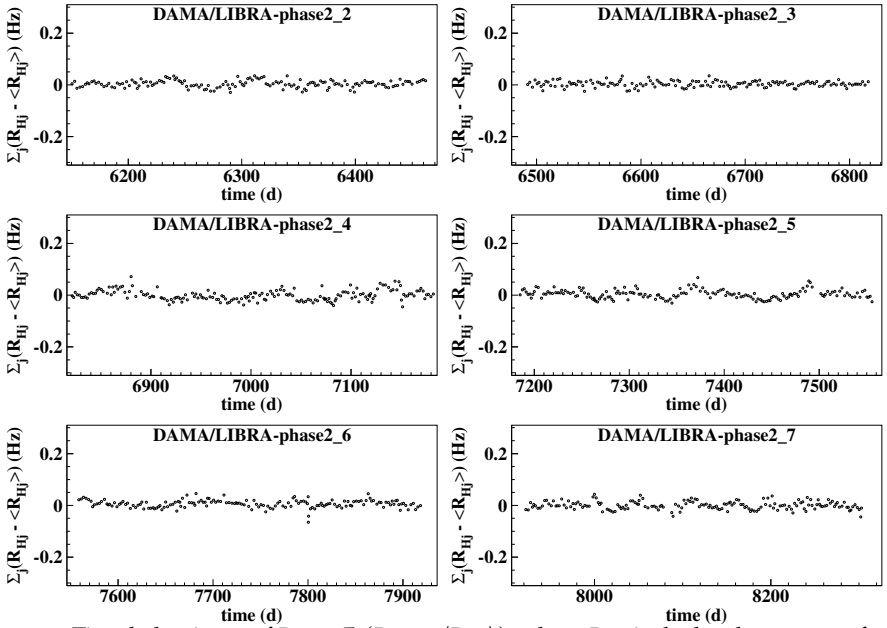

Fig. 2.16. Time behaviours of $R_H = \Sigma_j(R_{Hj} - \langle R_{Hj}\rangle)$, where R_{Hj} is the hardware rate of each detector above single photoelectron threshold (that is including the noise), j identifies the detector and $\langle R_{Hj}\rangle$ is the mean value of R_{Hj} in the corresponding annual cycle.

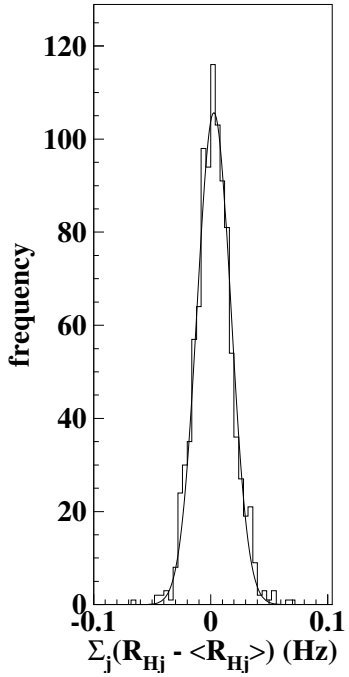

Fig. 2.17. Distribution of R_H during the DAMA/LIBRA–phase2 annual cycles (histogram); the superimposed curve is a gaussian fit.

2.6.3 The calibration factor

In long term running conditions the periodical calibrations are performed every $\simeq 10$ days with ^{241}Am source [1]. Although it is highly unlikely that a variation of the calibration factor (proportionality factor between the area of the recorded pulse and the energy), tdcal, could play any role, a quantitative investigation on that point has been carried out.

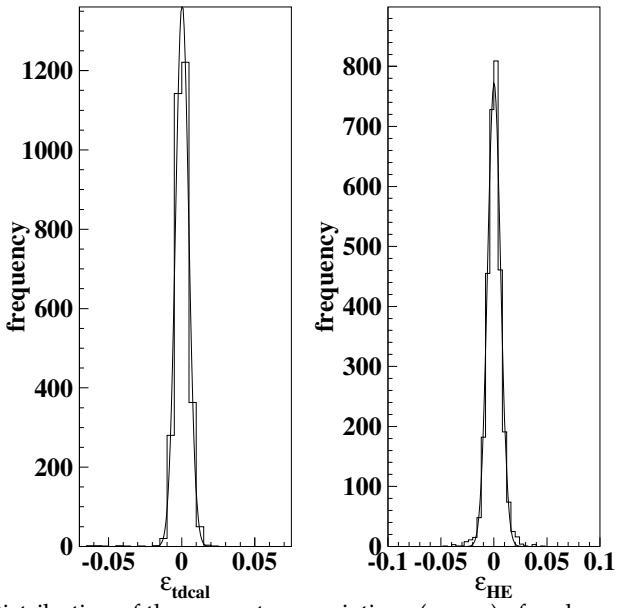

Fig. 2.18. *Left:* Distribution of the percentage variations (ϵ_{tdcal}) of each energy scale factor (tdcal) with respect to the value measured in the previous calibration (histogram); the standard deviation is 0.5%. *Right:* Distribution of the percentage variations (ϵ_{HE}) of the high energy scale factor with respect to the mean values (histogram); the standard deviation is 0.6%. The panels refer to the DAMA/LIBRA–phase2 annual cycles and the superimposed curves are gaussian fits.

For this purpose, we define the percentage variation of each energy scale factor (tdcal) with respect to the value measured in the previous calibration: $\epsilon_{tdcal} = \frac{tdcal_k - tdcal_{k-1}}{tdcal_{k-1}}$ (here $tdcal_k$ is the value of the calibration factor in the k-th calibration). The distribution of ϵ_{tdcal} for all the detectors during the DAMA/LIBRA–phase2 annual cycles is given in Fig. 2.18–*Left*. This distribution shows a gaussian behaviour with $\sigma \simeq 0.5\%$. Since the results of the routine calibrations are properly taken into account in the data analysis, such a result allows us to conclude that the energy calibration factor for each detector is known with an uncertainty $\ll 1\%$ during the data taking periods.

Moreover, the distribution of the percentage variations (ϵ_{HE}) of the high energy scale factor with respect to the mean values for all the detectors and for the DAMA/LIBRA–phase2 annual cycles is reported in Fig. 2.18–*right*. Also this distribution shows a gaussian behaviour with $\sigma \simeq 0.6\%$.

As also discussed in Ref. [2,15,16], the possible variation of the calibration factor for each detector during the data taking would give rise to an additional energy spread (σ_{cal}) besides the detector energy resolution (σ_{res}). The total energy spread can be, therefore, written as: $\sigma = \sqrt{\sigma_{res}^2 + \sigma_{cal}^2} \simeq \sigma_{res} \cdot [1 + \frac{1}{2} \cdot (\frac{\sigma_{cal}}{\sigma_{res}})^2]$; clearly the contribution due to the calibration factor variation is negligible since $\frac{1}{2} \cdot (\frac{\sigma_{cal}/E}{\sigma_{res}/E})^2 \lesssim 7.5 \times 10^{-4} \frac{E}{20keV}$ (where the adimensional ratio $\frac{E}{20keV}$ accounts for the energy dependence of this limit value). This order of magnitude is confirmed by a MonteCarlo calculation, which credits – as already reported in Ref. [2,15,16] – a maximum value of the effect of similar variations of $tdcal$ on the modulation amplitude equal to $1 - 2 \times 10^{-4}$ cpd/kg/keV. Thus, also the unlikely idea that the calibration factor could play a role can be safely ruled out.

2.6.4 The efficiencies

The behaviour of the overall efficiencies during the whole data taking periods has been investigated. Their possible time variation depends essentially on the stability of the efficiencies related to the adopted acceptance windows; they are regularly measured by dedicated calibrations [1].

In particular, Fig. 2.19 shows the percentage variations of the efficiency values in the (1-8) keV energy interval for DAMA/LIBRA–phase2. They show a gaussian distribution with σ = 0.3%. Moreover, we have verified that the time behaviour of these percentage variations does not show any modulation with period and phase expected for a possible DM signal. In Table 2.3 the modulation amplitudes of the efficiencies in each energy bin between 1 and 10 keV are reported, showing that they are all consistent with zero. In particular, modulation amplitudes – considering the six DAMA/LIBRA–phase2 annual cycles all together – equal to $-(0.10 \pm 0.32) \times 10^{-3}$ and $(0.00 \pm 0.41) \times 10^{-3}$ are found for the (1-4) keV and (4-6) keV energy bins, respectively; both consistent with zero. Thus, also the unlikely idea of a possible role played by the efficiency is ruled out.

Energy	Modulation amplitudes ($\times 10^{-3}$)					
(keV)	LIBRA-ph2-2	LIBRA-ph2-3	LIBRA-ph2-4	LIBRA-ph2-5	LIBRA-ph2-6	LIBRA-ph2-7
1-4	$-(0.8 \pm 0.7)$	(0.7 ± 0.8)	(0.9 ± 0.8)	$-(1.3 \pm 0.8)$	$-(0.1 \pm 0.8)$	(0.2 ± 0.8)
4-6	(0.9 ± 1.0)	(0.9 ± 1.0)	$-(1.3 \pm 1.0)$	(0.5 ± 1.0)	$-(1.0 \pm 1.1)$	$-(0.2 \pm 1.0)$
6-8	(0.8 ± 0.8)	$-(0.7 \pm 0.7)$	(0.6 ± 0.8)	$-(0.1 \pm 0.8)$	$-(1.1 \pm 0.8)$	(0.5 ± 0.8)
8-10	$-(0.3 \pm 0.6)$	$-(0.5 \pm 0.5)$	$-(0.5 \pm 0.5)$	$-(0.3 \pm 0.5)$	(0.4 ± 0.6)	(0.3 ± 0.6)

Table 2.3. Modulation amplitudes obtained by fitting the time behaviour of the efficiencies including a cosine modulation with phase and period as for DM particles for the DAMA/LIBRA–phase2 annual cycles.

2.6.5 The background

In order to verify the absence of any significant background modulation, the energy distribution measured during the data taking periods in energy regions not

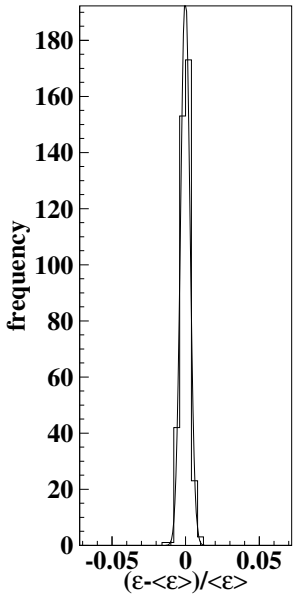

Fig. 2.19. Percentage variations of the overall efficiency values with the respect to their mean values for DAMA/LIBRA–phase2 (histogram); the superimposed curve is a gaussian fit.

of interest for DM detection has been investigated. The presence of background (of whatever nature) modulation is already excluded by the results on the measured rate integrated above 90 keV, R_{90}, as a function of the time; the latter one not only does not show any modulation, but allows one to exclude the presence of a background modulation in the whole energy spectrum at a level some orders of magnitude lower than the annual modulation observed in the *single-hit* events in the (1–6) keV energy region.

A further relevant support is given by the result of the analysis of the *multiple-hit* events which independently proofs that there is no modulation at all in the background event in the same energy region where the *single-hit* events present an annual modulation satisfying all the requirements of the DM annual modulation signature.

These results obviously already account for whatever kind of background including that possibly induced by neutrons, by Radon and by side reactions.

... more on Radon The DAMA/LIBRA detectors are excluded from the air of the underground laboratory by a 3-level sealing system [1]; in fact, this air contains traces of the radioactive Radon gas (^{222}Rn – $T_{1/2}$ = 3.82 days – and of ^{220}Rn – $T_{1/2}$ = 55 s – isotopes, which belong to the ^{238}U and ^{232}Th chains, respectively), whose daughters attach themselves to surfaces by various processes. In particular: i) the walls, the floor and the top of the inner part of the installation are insulated by Supronyl (permeability: 2×10^{-11} cm^2/s [36]) and a large flux of HP Nitrogen is released in the closed space of this inner part of the barrack housing the set-up. An Oxygen level alarm informs the operator before entering it, when necessary; ii)

the whole passive shield is sealed in a Plexiglas box and maintained continuously in HP Nitrogen atmosphere in slight overpressure with respect to the environment as well as the upper glove box for calibrating the detectors; iii) the detectors are housed in an inner sealed Cu box also maintained continuously in HP Nitrogen atmosphere in slight overpressure with respect to the environment; the Cu box can enter in contact only with the upper glove box – during calibrations – which is also continuously maintained in HP Nitrogen atmosphere in slightly overpressure with respect to the external environment.

Notwithstanding the above considerations, the Radon in the installation outside the Plexiglas box, containing the passive shield, is continuously monitored; it is at level of sensitivity of the used Radon-meter as reported in Fig. 2.20. Table 2.2 has already shown that no modulation of Radon is present in the environment of the set-up; moreover, the detectors are further isolated by the other two levels of sealing [1].

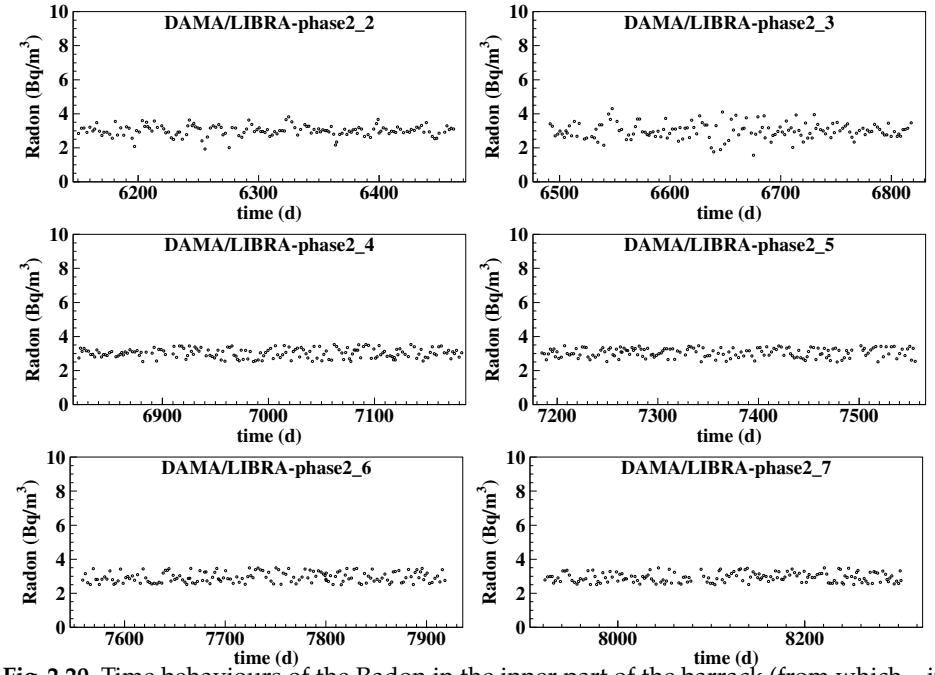

Fig. 2.20. Time behaviours of the Radon in the inner part of the barrack (from which – in addition - the detectors are further isolated by other two levels of sealing [1]) during the DAMA/LIBRA–phase2 annual cycles. The measured values are at the level of sensitivity of the used Radon-meter.

In Fig. 2.21 the distributions of the relative variations of the HP Nitrogen flux in the inner Cu box housing the detectors and of the pressure of it are shown as measured during the DAMA/LIBRA–phase2 annual cycles (the typical flux mean value for each annual cycle is of order of $\simeq$ 320 l/h and the typical overpressure mean value is of order of 3.1 mbar).

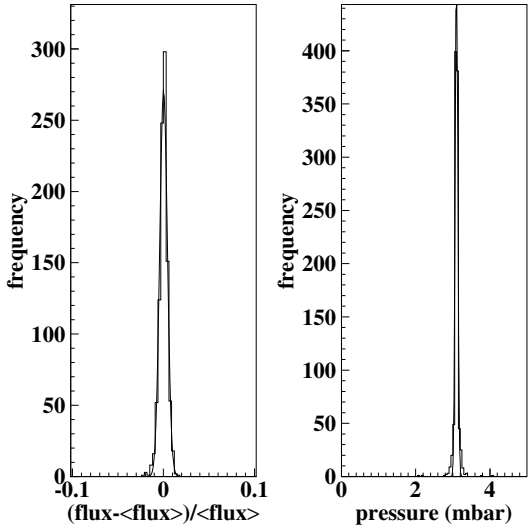

Fig. 2.21. Distributions of the HP Nitrogen flux in the inner Cu box housing the detectors and of the pressure of it as measured during the DAMA/LIBRA–phase2 annual cycles (histograms); the superimposed curves are gaussian fits. For clarity the HP Nitrogen flux has been given in terms of relative variations.

Possible Radon trace in the HP Nitrogen atmosphere inside the Cu box, housing the detectors, has been searched through the double coincidences of the gamma-rays (609 and 1120 keV) from ^{214}Bi Radon daughter, obtaining an upper limit on the possible Radon concentration in the Cu box HP Nitrogen atmosphere: $< 5.8 \times 10^{-2}$ Bq/m^3 (90% C.L.) [2]. Thus, a rate roughly $< 2.5 \times 10^{-5}$ cpd/kg/keV can be expected from this source at low energy. This shows that even an hypothetical, e.g. 10%, modulation of possible Radon in the HP Nitrogen atmosphere of the Cu box, housing the detectors, would correspond to a modulation amplitude $< 2.5 \times 10^{-6}$ cpd/kg/keV (< 0.01% of the observed modulation amplitude).

Moreover, it is worth noting that, while the possible presence of a sizeable quantity of Radon nearby a detector would forbid the investigation of the annual modulation signature (since every Radon variation would induce both the variation in the whole energy distribution and the continuous pollution of the exposed surfaces by the non-volatile daughters), it cannot mimic the DM annual modulation signature in experiments such as the former DAMA/NaI and DAMA/LIBRA–phase1 and the present DAMA/LIBRA–phase2 which record the whole energy distribution; in fact, possible presence of Radon variation can easily be identified in this case and some of the six requirements of the DM annual modulation signature would fail.

In conclusion, no significant role is possible from the Radon.

... more on side processes As mentioned, possible side reactions have also been carefully investigated and none able to mimic the exploited signature is available;

previous results on the topics hold (see e.g. Ref. [5], and references therein). In particular, the case of neutrons, muons and solar neutrinos has been discussed in details in Ref. [7,8], where it has been demonstrated that they cannot give any significant contribution to the DAMA annual modulation result. Table 2.6.5 summarizes the safety upper limits on the contributions to the observed modulation amplitude due to the total neutron flux at LNGS, either from (α, n) reactions, from fissions and from muons and solar-neutrinos interactions in the rocks and in the lead around the experimental set-up; the direct contributions of muons and solar neutrinos are reported there too. Not only the limits are quantitatively marginal, but none of such contributions is able to simultaneously satisfy all the requirements of the exploited signature. Other arguments can be found in Ref. [1–4,7,5,11,8,16,17,15].

	Source	$\Phi_{0,k}^{(n)}$ (neutrons cm^{-2} s^{-1})	η_k	t_k	$R_{0,k}$ (cpd/kg/keV)	$A_k = R_{0,k}\eta_k$ (cpd/kg/keV)	A_k/S_m^{exp}
SLOW neutrons	thermal n ($10^{-2} - 10^{-1}$ eV)	1.08×10^{-6}	$\simeq 0$ however $\ll 0.1$	–	$< 8 \times 10^{-6}$	$\ll 8 \times 10^{-7}$	$\ll 7 \times 10^{-5}$
	epithermal n (eV-keV)	2×10^{-6}	$\simeq 0$ however $\ll 0.1$	–	$< 3 \times 10^{-3}$	$\ll 3 \times 10^{-4}$	$\ll 0.03$
FAST neutrons	fission, $(\alpha, n) \to n$ (1-10 MeV)	$\simeq 0.9 \times 10^{-7}$	$\simeq 0$ however $\ll 0.1$	–	$< 6 \times 10^{-4}$	$\ll 6 \times 10^{-5}$	$\ll 5 \times 10^{-3}$
	$\mu \to n$ from rock (> 10 MeV)	$\simeq 3 \times 10^{-9}$	0.0129	end of June	$\ll 5 \times 10^{-4}$	$\ll 7 \times 10^{-6}$	$\ll 6 \times 10^{-4}$
	$\mu \to n$ from Pb shield (> 10 MeV)	$\simeq 6 \times 10^{-9}$	0.0129	end of June	$\ll 1.1 \times 10^{-3}$	$\ll 1.4 \times 10^{-5}$	$\ll 1.3 \times 10^{-3}$
	$\nu \to n$ (few MeV)	$\simeq 3 \times 10^{-10}$	0.03342*	Jan. 4th*	$\ll 5 \times 10^{-5}$	$\ll 1.8 \times 10^{-6}$	$\ll 1.6 \times 10^{-4}$
	direct μ	$\Phi_0^{(\mu)} \simeq 20\ \mu\ m^{-2}d^{-1}$	0.0129	end of June	$\simeq 10^{-7}$	$\simeq 10^{-9}$	$\simeq 10^{-7}$
	direct ν	$\Phi_0^{(\nu)} \simeq 6 \times 10^{10}\ \nu\ cm^{-2}s^{-1}$	0.03342*	Jan. 4th*	$\simeq 10^{-5}$	3×10^{-7}	3×10^{-5}

Table 2.4. Summary of the contributions to the total neutron flux at LNGS; the value, $\Phi_{0,k}^{(n)}$, the relative modulation amplitude, η_k, and the phase, t_k, of each component is reported. It is also reported the counting rate, $R_{0,k}$, in DAMA/LIBRA–phase2 for *single-hit* events, in the $(1 - 6)$ keV energy region induced by neutrons, muons and solar neutrinos, detailed for each component. The modulation amplitudes, A_k, are reported as well, while the last column shows the relative contribution to the annual modulation amplitude observed by DAMA/LIBRA–phase2, $S_m^{exp} \simeq 0.011$ cpd/kg/keV. For details see Ref. [8] and references therein.

* The annual modulation of solar neutrino is due to the different Sun-Earth distance along the year; so the relative modulation amplitude is twice the eccentricity of the Earth orbit and the phase is given by the perihelion.

2.6.6 Conclusions on possible systematics effects and side reactions

No modulation has been found in any possible source of systematics or side reactions; thus, upper limits (90% C.L.) on the possible contributions to the DAMA/LIBRA–phase2 measured modulation amplitude are summarized in Table

2.5. In particular, they cannot account for the measured modulation both because quantitatively not relevant and unable to mimic the observed effect.

Source	Main comment (see also Ref. [1])	Cautious upper limit (90%C.L.)
Radon	Sealed Cu Box in HP Nitrogen atmosphere, 3-level of sealing	$< 2.5 \times 10^{-6}$ cpd/kg/keV
Temperature	Air conditioning + huge heat capacity	$< 10^{-4}$ cpd/kg/keV
Noise	Efficient rejection	$< 10^{-4}$ cpd/kg/keV
Energy scale	Routine + intrinsic calibrations	$< 1 - 2 \times 10^{-4}$ cpd/kg/keV
Efficiencies	Regularly measured	$< 10^{-4}$ cpd/kg/keV
Background	No modulation above 6 keV; no modulation in the (1 – 6) keV *multiple-hit* events; this limit includes all possible sources of background	$< 10^{-4}$ cpd/kg/keV
Side reactions	From muon flux variation measured by MACRO	$< 3 \times 10^{-5}$ cpd/kg/keV
In addition: no effect can mimic the signature		

Table 2.5. Summary of the results obtained by investigating possible sources of systematics or of side reactions in the data of the DAMA/LIBRA–phase2 annual cycles. None able to give a modulation amplitude different from zero has been found; thus cautious upper limits (90% C.L.) on the possible contributions to the measured modulation amplitude have been calculated and are shown here.

2.7 Conclusions

The data of the new DAMA/LIBRA–phase2 confirm a peculiar annual modulation of the *single-hit* scintillation events in the (1–6) keV energy region satisfying all the many requirements of the DM annual modulation signature; the cumulative exposure by the former DAMA/NaI, DAMA/LIBRA–phase1 and DAMA/LIBRA–phase2 is 2.46 ton $\times$ yr.

As required by the exploited DM annual modulation signature: 1) the *single-hit* events show a clear cosine-like modulation as expected for the DM signal; 2) the measured period is equal to (0.999 ± 0.001) yr well compatible with the 1 yr period as expected for the DM signal; 3) the measured phase (145 ± 5) days is compatible with the roughly $\simeq 152.5$ days expected for the DM signal; 4) the modulation is present only in the low energy (1–6) keV interval and not in other

higher energy regions, consistently with expectation for the DM signal; 5) the modulation is present only in the *single-hit* events, while it is absent in the *multiple-hit* ones as expected for the DM signal; 6) the measured modulation amplitude in NaI(Tl) target of the *single-hit* scintillation events in the (2–6) keV energy interval, for which data are also available by DAMA/NaI and DAMA/LIBRA–phase1, is: (0.0103 ± 0.0008) cpd/kg/keV (12.9 σ C.L.). No systematic or side processes able to mimic the signature, i.e. able to simultaneously satisfy all the many peculiarities of the signature and to account for the whole measured modulation amplitude, has been found or suggested by anyone throughout some decades thus far. In particular, arguments related to any possible role of some natural periodical phenomena have been discussed and quantitatively demonstrated to be unable to mimic the signature (see e.g. Ref. [7,8]). Thus, on the basis of the exploited signature, the model independent DAMA results give evidence at 12.9 σ C.L. (over 20 independent annual cycles and in various experimental configurations) for the presence of DM particles in the galactic halo.

In order to perform corollary investigation on the nature of the DM particles in given scenarios, model-dependent analyses are necessary[3]; thus, many theoretical and experimental parameters and models are possible and many hypotheses must also be exploited. In particular, the DAMA model independent evidence is compatible with a wide set of astrophysical, nuclear and particle physics scenarios for high and low mass candidates inducing nuclear recoil and/or electromagnetic radiation, as also shown in a wide literature. Moreover, both the negative results and all the possible positive hints, achieved so-far in the field, can be compatible with the DAMA model independent DM annual modulation results in many scenarios considering also the existing experimental and theoretical uncertainties; the same holds for indirect approaches. For a discussion see e.g. Ref. [5] and references therein. Model dependent analyses, to update the allowed regions in various scenarios and to enlarge the investigations to other ones, will be presented elsewhere.

Finally, we stress that to efficiently disentangle among the many possible candidates and scenarios an increase of exposure in the new lowest energy bin is important. The experiment is collecting data and related R&D is under way.

References

1. R. Bernabei et al., Nucl. Instr. and Meth. A **592**, 297 (2008).
2. R. Bernabei et al., Eur. Phys. J. C **56**, 333 (2008).
3. R. Bernabei et al., Eur. Phys. J. C **67**, 39 (2010).
4. R. Bernabei et al., Eur. Phys. J. C **73**, 2648 (2013).
5. R. Bernabei et al., Int. J. of Mod. Phys. A **28**, 1330022 (2013).
6. R. Bernabei et al., J. of Instr. **7**, P03009 (2012).
7. R. Bernabei et al., Eur. Phys. J. C **72**, 2064 (2012).
8. R. Bernabei et al., Eur. Phys. J. C **74**, 3196 (2014).

[3] It is worth noting that it does not exist in direct and indirect DM detection experiments approaches which can offer such information independently on assumed models.

9. DAMA coll., issue dedicated to DAMA, Int. J. of Mod. Phys. A **31** (2016) and references therein.
10. for complete references: http://people.roma2.infn.it/dama/web/publ.html
11. R. Bernabei et al., Eur. Phys. J. C **74**, 2827 (2014).
12. R. Bernabei et al., *arXiv:1805.10486*.
13. P. Belli, R. Bernabei, C. Bacci, A. Incicchitti, R. Marcovaldi, D. Prosperi, DAMA proposal to INFN Scientific Committee II, April 24^{th} 1990.
14. R. Bernabei et al., Il Nuovo Cim. A **112**, 545 (1999).
15. R. Bernabei et al., Eur. Phys. J. C **18**, 283 (2000).
16. R. Bernabei el al., La Rivista del Nuovo Cimento **26** n.1, 1-73 (2003), and references therein.
17. R. Bernabei et al., Int. J. Mod. Phys. D **13**, 2127 (2004) and references therein.
18. K.A. Drukier et al., Phys. Rev. D **33**, 3495 (1986).
19. K. Freese et al., Phys. Rev. D **37**, 3388 (1988).
20. R. Bernabei and A. Incicchitti, Int. J. Mod. Phys. A **32**, 1743007 (2017).
21. D. Smith and N. Weiner, Phys. Rev. D **64**, 043502 (2001).
22. D. Tucker-Smith and N. Weiner, Phys. Rev. D **72**, 063509 (2005).
23. D. P. Finkbeiner et al, Phys. Rev. D **80**, 115008 (2009).
24. K. Freese et al., Phys. Rev. D **71**, 043516 (2005).
25. K. Freese et al., Phys. Rev. Lett. **92**, 111301 (2004).
26. P. Belli et al., Int. J. of Mod. Phys. A **31**, 1642005 (2016).
27. R. Bernabei et al., Eur. Phys. J. C **47**, 263 (2006).
28. P. Gondolo et al., New Astron. Rev. **49**, 193 (2005).
29. G. Gelmini and P. Gondolo, Phys. Rev. D **64**, 023504 (2001).
30. F.S. Ling, P. Sikivie and S. Wick, Phys. Rev. D **70**, 123503 (2004).
31. G. Ranucci and M. Rovere, Phys. Rev. D **75**, 013010 (2007).
32. J.D. Scargle, Astrophys. J. **263**, 835 (1982).
33. W.H. Press et al., "Numerical recipes in Fortran 77: the art of scientific computing", Cambridge University Press, Cambridge, England 1992, section 13.8.
34. J.H. Horne and S.L. Baliunas, Astrophys. J. **302**, 757 (1986).
35. W.T. Eadie et al., "Statistical methods in experimental physics", ed. American Elsevier Pub. (1971).
36. M. Wojcik, Nucl. Instrum. and Meth. B **61**, 8 (1991).